The Structure of a Moving Vortex Lattice

D. W. Braun, G. W. Crabtree, H. G. Kaper, A. E. Koshelev,*
G. K. Leaf, D. M. Levine, V. M. Vinokur
Argonne National Laboratory, Argonne, IL 60439
(MCS-P537-0895, December 1995)

Abstract

Numerical solutions of the time-dependent Ginzburg-Landau equations show a new mechanism for plastic motion of a driven vortex lattice in a clean superconductor. The mechanism, which involves the creation of a defect superstructure, is intrinsic to the moving vortex lattice and is independent of bulk pinning. Other structural features found in the solutions include a reorientation of the vortex lattice and a gradual healing of lattice defects under the influence of a transport current.

PACS numbers: 74.60.Ge

*Also: Institute of Solid State Physics, Chernogolovka, Moscow District, 142432, Russia.

Recently, attention has focused increasingly on the dynamic states of a vortex system. Much of the interest concerns the type of motion of a vortex lattice under an applied current [1–3]. It has been observed that, in a significant region of the phase diagram below the vortex lattice melting line, vortex motion is predominantly plastic motion. The explanation given in [1,2] relies heavily on the notion that the vortex interactions compete with a randomness in the driven vortex system [4,5]. In this Letter, we present the results of a numerical study of the motion of a vortex lattice in a clean finite sample and find a different mechanism for plastic vortex motion. Past considerations excluded the effects of the current-induced magnetic field. We show that a current increases the vortex spacing in the direction of vortex motion and enforces the formation of *fault lines* to accomodate the resulting strains. The fault lines serve as a source of plastic deformations. The mechanism is the result of the intrinsic behavior of the vortex lattice and is independent of bulk pinning. It may be responsible for plastic motion in very clean superconductors.

The structure of a vortex lattice moving under the influence of a transport current in a homogeneous superconducting sample depends on the relative strengths of the Lorentz force and the barrier forces associated with the free surfaces [6]. Numerical solutions of the time-dependent Ginzburg-Landau (TDGL) equations [7] show that the barrier forces dominate at weak currents. Vortex motion is confined to the interior of the sample, and the vortex lattice is essentially static. Its close-packed rows align with the free surfaces. The lattice structure may have defects, whose origin can be traced to the transient phase, but these defects disappear gradually, and a more or less uniform structure with isolated defects remains. When the Lorentz force dominates, vortices enter and leave through the free surfaces, and the entire vortex lattice moves steadily. The lattice structure changes in two ways. We see a change in the orientation of the lattice, where the close-packed rows align with the direction of the Lorentz force, and the development of a defect superstructure, where one or several distinct "fault lines" separate regions of approximately uniform structure. A fault line consists of several aligned dislocations and finite segments of a 30° boundary. The fault lines remain more or less stationary as the lattice moves. They provide the principal mechanism supporting the vortex density gradient induced by the self-field of the current and serve as a source of plastic deformations. Similar defect structures have been observed in decorations of static vortex lattices with density gradients [8,9].

The computations, described in detail in [10,11], were done for a rectangular homogeneous pin-free superconducting sample, infinite in z, periodic in y, and bounded in x. The magnetic field is in the positive z direction. A transport current J in the positive y direction is induced by a field differential between the free surfaces: $H_l = H_0 + \Delta H$, $H_r = H_0 - \Delta H$, where $\Delta H = \frac{1}{2}J$. The resulting Lorentz force acts in the positive x direction. Lengths are measured in units of the penetration depth λ; time in units of ξ^2/D (ξ the coherence length, D the normal diffusion coefficient); fields in units of $H_c\sqrt{2}$ (H_c the thermodynamic critical field); and current densities in units of $(cH_c\sqrt{2})/(4\pi\lambda)$. Unless otherwise noted, all results refer to a standard configuration: cross section 32×48 in the (x, y) plane, Ginzburg-Landau parameter $\kappa = 4$, and a magnetic field with $H_0 = 0.8$ and $\Delta H = 0$ (no current), 0.125 ("weak" current), 0.250 ("intermediate" current), or 0.500 ("strong" current). The corresponding current densities are approximately 0, 2, 4, and 8% of the BCS depairing-current density.

Starting from the Meissner state, we increase the applied field to $H_0 = 0.8$, apply the

transport current as appropriate, and let the system evolve through the transient phase before we begin recording data. The average number of vortices in the steady state varies from 230 (no current) to 660 (strong current). The position of every vortex is determined from the solution of the TDGL equations. The structure and evolution of the vortex lattice are analyzed by means of a Delauney triangulation [12], which is constructed at each recorded time step. Each vortex in the bulk with fewer or more than six neighbors is identified with a defect in the lattice. The computational results for the standard configuration are summarized in Figs. and .

In the absence of a transport current, 230 vortices enter the sample to form a dilute vortex structure with an average lattice spacing $a_0 = 2.58\lambda$. The average magnetic induction in the sample is $B = 0.27$, considerably less than the applied field $H_0 = 0.8$. The lattice is static. Its structure remains defective; the major types of defects are isolated dislocations (pairs of defects—one with five, the other with seven neighbors) and finite segments of 30° boundaries (strings of three or more contiguous dislocations). The vortex region is separated from the free surfaces by a vortex-free region, 2.1λ wide. The Meissner current flows entirely within these vortex-free regions.

A weak current ($\Delta H = 0.125$) almost doubles the average number of vortices to 459. The vortices form an almost ideal crystal structure, with $a_0 = 1.88\lambda$. The lattice is again static, but slightly displaced to the right edge. The supercurrent density at the left edge of the sample is approximately equal to the BCS depairing-current density. The close-packed direction of the lattice is again aligned with the free surfaces. The remaining defects are the remnants of a misoriented grain in the center of the sample, whose origin goes back to the transient phase and which gradually heals during the recording period.

At the intermediate current ($\Delta H = 0.250$), the surface barrier at the right edge is broken, and the lattice moves steadily in the positive x direction. At the left edge, vortices penetrate into the sample in a highly organized manner: A penetrating vortex triggers successive nucleations, which propagate along the surface of the sample in the direction of the current ("zipper" penetration). Vortices exit through the right surface, where the vortex-free region has disappeared completely. The average number of vortices in the sample increases to approximately 565; this number oscillates in time, but the amplitude of the oscillation is always less than 1%. The close-packed direction of the moving lattice is oriented along the direction of motion. A reorientation of a moving vortex lattice was observed in early experiments [13] and, more recently, in YBCO [14]. A mechanism for the reorientation in the presence of bulk pinning was proposed in the context of collective pinning theory in [15]. Our investigation indicates that the reorientation also can be caused by the free surfaces of the sample. Approximately one third of the transport current now flows in the interior the sample, supporting the steady motion of the lattice. The resulting small gradient in the vortex density leads to an expansion of the lattice as x increases.

The critical current, at which the vortex lattice first moves, can be estimated. As long as $H_l > H_{\max}(B)$ ($H_r < H_{\min}(B)$), vortices will break through the free surface at the left (right) edge and enter (leave) the sample, thus increasing (decreasing) the magnetic induction just inside the sample until it reaches the value B_l (B_r) for which $H_l = H_{\max}(B_l)$ ($H_r = H_{\min}(B_r)$); see [16–18]. Approximate (dimensionless) expressions for $H_{\max}(B)$ and $H_{\min}(B)$ in the range $H_{c1} < B < H_{c2}$ are

$$H_{\max}(B) \approx \left(B^2 + H_p^2\right)^{1/2}, \; H_{\min}(B) \approx B - B_0, \tag{1}$$

where $B_0 = (2\pi\sqrt{3})/(48\kappa)$ [17]. Usually, it is assumed that $H_p = H_c$.

Figure (left inset) shows the computed values of (H_l, B_l) and (H_r, B_r) for various currents. A best fit of a curve $H = H_{\max}(B)$ through the data (H_l, B_l) for no current, weak current, and intermediate current yields $H_p \approx 0.78$; hence, our computations suggest that the penetration field in the Meissner state is $H_p \approx 1.1 H_c$. The dashed line is the graph of $H_{\max}$ with $H_p = 0.78$. It represents the stability boundary for the left surface. The data (H_l, B_l) for a strong current (discussed below) lie very close to the critical curve $H = H_{\max}(B)$—an indication that the expression for $H_{\max}(B)$ remains a good approximation when the lattice moves faster. The solid line is the graph of $H_{\min}$ for $\kappa = 4$. It represents the stability boundary for the right surface. The data (H_r, B_r) for no current and weak current lie below the graph—an indication that the surface barrier at the right edge has not been broken and the lattice is stationary. The data (H_r, B_r) for the intermediate and strong current lie on the line $B = H$. The surface barrier at the right edge of the sample has been broken, and the barrier force has no effect on the moving lattice.

The critical current $J_{\rm cr}$, at which the surface barrier is first broken, can be estimated from Eq. (1),

$$J_{\rm cr} = 2(\Delta H)_{\rm cr} = \frac{H_p^2}{2H_0 + B_0} + B_0. \tag{2}$$

For $H_0 = 0.8$, we find $J_{\rm cr} \approx 0.42$. Computations with $\Delta H = 0.175, 0.195, 0.200$ show that vortices first break through the surface barrier when $\Delta H = 0.200$. The magnetic induction profile and the data (H_l, B_l), (H_r, B_r) for the critical current are included in Fig. . Also included in Fig. (right inset) is a blow-up of the field profile for the critical current near the right edge of the sample. As predicted by Eq. 1, the value of B_r exceeds H_r by the small positive quantity B_0. This result resolves the discrepancy about the sign of the correction in [17,18].

When the lattice moves steadily across the sample, the total current J splits into a surface contribution, J_s, and a bulk contribution, J_b. The self-field of the bulk current induces a gradient of the magnetic induction and, therefore, a gradient of the vortex density, and this gradient leads in turn to a deformation of the lattice.

The field profile in the bulk can be found from the force balance equation for the overdamped steadily moving elastic vortex lattice. In the case of uniaxial compression in the x direction, this equation reduces to $-C_{11}(1/B)(\mathrm{d}B/\mathrm{d}x) = \gamma/(8\pi)$, where γ is a constant and C_{11} is the bulk modulus, $C_{11}(B) \approx (B^2/(4\pi))(1 - 1/(4\kappa B))$. The differential equation can be integrated, for example, from the right edge, where $B = B_r$, into the bulk. The constant γ is then determined by the condition that the field at the left edge of the bulk is $B = B_l$. Identifying the width of the bulk with the width of the sample, d, we find the following expression for the magnetic field in the bulk:

$$B(x) = \frac{1}{4\kappa} + \left(\left(B_r - \frac{1}{4\kappa}\right)^2 + \gamma d\left(1 - \frac{x}{d}\right)\right)^{1/2}, \tag{3}$$

where $\gamma d = (B_l - B_r)(B_l + B_r - 1/(2\kappa))$. Substitution of the expressions $B_r = H_r = H_0 - \frac{1}{2}J$ and $B_l = H_l - J_s = H_0 + \frac{1}{2}J - J_s$ gives $B(x)$ in terms of H_0, J, and J_s. The dashed lines in Fig. show the excellent agreement with the field profiles found in the computations.

We proceed to the case of the strong transport current, $\Delta H = 0.500$. The self-field of the current inside the sample induces a significant density gradient: The density near the left edge is approximately three times the density near the right edge. The lattice experiences a significant strain in the left part of the sample. Slightly beyond the center, it can no longer bear the strain, and plastic deformation occurs. A defect boundary ("fault line") appears, which consists of several aligned dislocations and finite segments of a 30° boundary. The fault line remains more or less stationary as the lattice moves across the sample. The critical strain $\varepsilon_{\rm pl}$, at which the lattice yields, can be estimated from the stretch in the horizontal bonds from the left edge to the fault line, $\varepsilon_{\rm pl} \approx 0.35$.

The current at which the lattice first shows plastic deformation, $J_{\rm pl}$, can be estimated. As long as the strain near the right edge of the sample, $\varepsilon_{xx} = (B_l - B_r)/B_l$, is less than the plastic limit for uniaxial stretching, $\varepsilon_{\rm pl}$, the lattice is deformed elastically throughout the bulk. The fault line first appears at the right edge when $B_l - B_r = \varepsilon_{\rm pl} B_l$. With $B_l - B_r = J_{\rm pl} - J_s$ and $B_l = H_0 + \frac{1}{2}J_{\rm pl} - J_s$, we find

$$J_{\rm pl} = \frac{(1 - \varepsilon_{\rm pl})J_s + \varepsilon_{\rm pl} H_0}{1 - \varepsilon_{\rm pl}/2}. \tag{4}$$

At stronger currents, plastic deformations appear at a finite distance $x_{\rm pl}$ from the left edge. This distance can be estimated from the relation $B_l - B(x_{\rm pl}) = \varepsilon_{\rm pl} B_l$. Using Eq. (3) for the field, we find

$$\frac{x_{\rm pl}}{d} = \varepsilon_{\rm pl} B_l \frac{(2 - \varepsilon_{\rm pl})B_l - 1/(2\kappa)}{(B_l - B_r)(B_l + B_r - 1/(2\kappa))}. \tag{5}$$

Here, $B_l - B_r = J - J_s$ and $B_l = H_0 + \frac{1}{2}J - J_s$.

The development of a stationary defect superstructure in a moving vortex lattice is one of the main findings of our computations. Further computations have shown that, in a wider sample, this superstructure is even more developed. The lattice structure at the final time step in a sample whose cross section in the (x, y) plane measured 48×32 in a strong current, ($H_0 = 1.05$, $\Delta H = 0.75$) is shown in Fig. . Several fault lines are necessary to support the large density differential across the sample. Note that the close-packed direction rotates each time a fault line is encountered.

Summarizing, we have shown a new mechanism for plastic motion of a driven vortex lattice in a clean superconductor. The mechanism involves the creation of a superstructure of lattice defects, which supports the gradient in the vortex density induced by the self-field of the current. Although the lattice moves across the sample, the defect superstructure remains static. We have also shown a dynamic reorientation of the lattice. When the current is weak, the lattice is essentially static, and its close-packed direction is aligned with the free surfaces. When the current exceeds a critical value, the lattice moves, and its close-packed direction is aligned with the direction of motion. Finally, we have shown a gradual healing of the lattice defects under the influence of a transport current.

This work was supported by the Mathematical, Information, and Computational Sciences Division subprogram of the Office of Computational and Technology Research and the Materials Sciences Office of the U.S. Department of Energy Basic Energy Sciences Program under Contract No. W-31-109-Eng-38, and by the National Science Foundation Office of the Science and Technology Center, under Contract No. DMR-91-20000.

References

[1] S. Bhattacharya and M. J. Higgins, Phys. Rev. Lett., **70**, 2617 (1993).

[2] W. K. Kwok et al., Phys. Rev. Lett., **73**, 2614 (1994).

[3] W. R. White, A. Kapitulnik, and M. R. Beasley, Phys. Rev. **B**, **50**, 6303 (1994) .

[4] S. N. Coppersmith, Phys. Rev. Lett., **65**, 1044 (1990).

[5] A. E. Koshelev and V. M. Vinokur, Phys. Rev. Lett., **73**, 3580 (1994).

[6] P. DeGennes, *Superconductivity in Metals and Alloys*. Benjamin, New York, 1966.

[7] A. Schmid, Phys. Kondens. Mater., **5**, 302 (1966); L. P. Gor'kov and G. M. Eliashberg, Zh. Eksp. Teor. Fiz., **54**, 612 (1968) [Sov. Phys. JETP **27**, 328 (1968)].

[8] U. Essmann and H. Träuble, Phys. Stat. Sol., **32**, 337 (1969).

[9] M. Marchevsky et al., Leiden University, preprint (1995).

[10] W. D. Gropp et al., J. Comp. Phys. (in press).

[11] D. W. Braun et al., Technical Memorandum ANL/MCS-TM-XXX, Mathematics and Computer Science Division, Argonne National Laboratory (1995).

[12] F. F. Preparata and M. L. Shamos, *Computational Geometry: An Introduction*. Springer-Verlag, New York, 1985.

[13] A. T. Fiory, Phys. Rev. Lett., **27**, 501 (1971).

[14] J. M. Harris, et al., Phys. Rev. Lett., **74**, 3685 (1995).

[15] A. Schmid and W. Hauger, J. Low Temp. Phys., **11**, 667 (1973).

[16] V. V. Shmidt, Zh. Eksp. Teor. Fiz. **61**, 398 (1971) [Sov. Phys. JETP **34**, 211 (1972)].

[17] F. F. Ternovskii and L. N. Shekhata, Zh. Eksp. Teor. Fiz. **62**, 2297 (1972) [Sov. Phys. JETP **35**, 1202 (1972)].

[18] J. R. Clem, in: *Proc. 13th Conf. on Low Temperature Physics* (LT 13), K. D. Timmerhaus, W. J. O'Sullivan, and E. F. Hammel, eds. Vol. 3, p. 102. Plenum, New York, 1974.

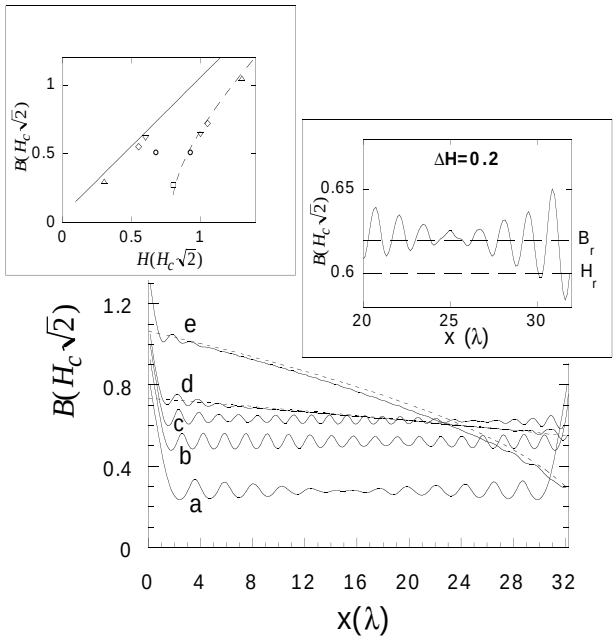

Fig. 1. Magnetic induction profiles (averaged over y) obtained from computations (solid lines) and theory (dashed lines); (a) no current, (b) weak current, (c) critical current, (d) intermediate current, (e) strong current. Left inset: Stability boundaries (see text) and computed values of (H_l, B_l) and (H_r, B_r); Dashed (solid) line: Stability boundary for left (right) free surface. Right inset: Magnetic induction profile near the right edge of the sample for critical current.

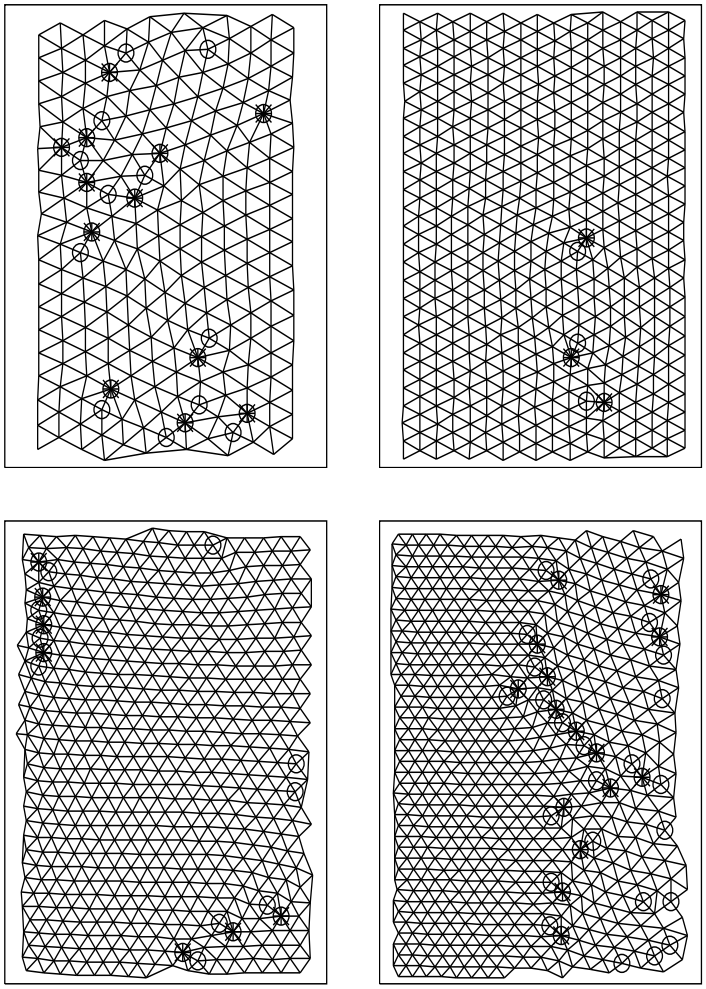

Fig. 2. Lattice structure in 32×48 sample (bulk only); $H_0 = 0.8$; lattice defects are marked. Top left: no current, top right: weak current, bottom left: intermediate current, bottom right: strong current.

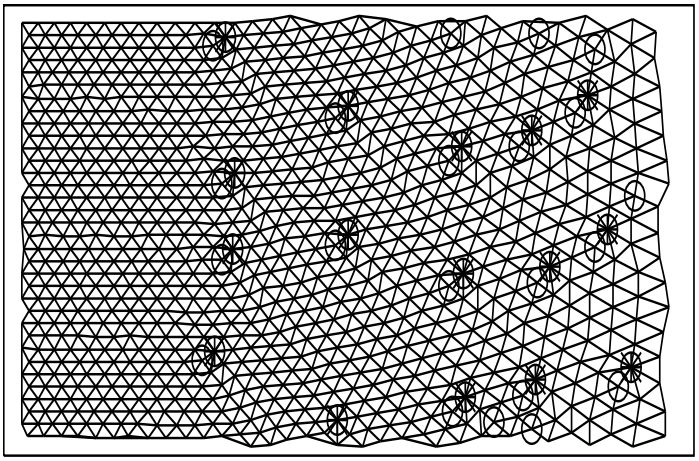

Fig. 3. Lattic structure in 48×32 sample (bulk only); $H_0 = 1.05$, $\Delta H = 0.75$; lattice defects are marked.